Supramolecular Chemistry
Publication details, including instructions for authors and subscription information:
http://www.informaworld.com/smpp/title~content=t713649759

Optical Characterization of Bio-assembled Hybrid Nanostructures

Joseph M. Slocik[a]; Alexander O. Govorov[b]; Rajesh R. Naik[a]
[a] Materials and Manufacturing Directorate, Air Force Research Laboratory, Wright-Patterson AFB, Dayton, OH, USA [b] Department of Physics and Astronomy, Ohio University, Athens, OH, USA

To cite this Article Slocik, Joseph M. , Govorov, Alexander O. and Naik, Rajesh R.(2006) 'Optical Characterization of Bio-assembled Hybrid Nanostructures', Supramolecular Chemistry, 18: 5, 415 — 421
To link to this Article: DOI: 10.1080/10615800600658925
URL: http://dx.doi.org/10.1080/10615800600658925

Supramolecular Chemistry, July–August 2006 Vol. 18 (5), pp. 415–421

Optical Characterization of Bio-assembled Hybrid Nanostructures

JOSEPH M. SLOCIK[a], ALEXANDER O. GOVOROV[b] and RAJESH R. NAIK[a,*]

[a]*Materials and Manufacturing Directorate, Air Force Research Laboratory, Wright-Patterson AFB, Dayton, OH 45433-7702, USA;* [b]*Department of Physics and Astronomy, Ohio University, Athens, OH 45701, USA*

(Received 27 November 2005; Accepted 24 February 2006)

Biological systems exemplify the utilization of highly specific recognition processes with a diverse set of building blocks for the synthesis and assembly of precisely defined nanomaterials. Consequently, these specialized biological processes and components are appealing for materials synthesis and have included the use of oligonucleotides, proteins, viruses, and antibodies as the primary organizational element. As a result, we present a peptide for gold reduction and synthesis, antibody recognition, and the antibody mediated assembly of gold/QDot nanostructures through a network of antibody-epitope and streptavidin/biotin interfaces. Optically, these structures exhibited increased quenching of fluorescence dependent on the number of attached gold particles. This was furthermore confirmed and consistent with theoretical calculations of exciton-energy transfer processes involving mixed numbers of gold particles per quantum dot.

Keywords: Exciton; Geometric; Electrostatic; Stereochemical; Bionanotechnology, Nanoparticles, Quantum dots; Gold, Flourescence

INTRODUCTION

Biological systems exhibit a paramount level of control in the synthesis and assembly of functional inorganic materials with respect to the overall prevailing chemistry and resultant properties. Examples include the ordering of magnetite particles in chains by magnetotactic bacteria [1], the exoskeleton construction of silica frustules by marine diatoms [2], and the architecture of abalone shells [3]. Collectively, these systems highlight the utilization of highly developed recognition processes (metal–protein recognition, protein–protein), complementarity (geometric, electrostatic, stereochemical), and a diverse set of building blocks (metal chelating peptides, proteins) to promote nanoparticle synthesis and assembly.

Presently, there is an increased interest in these specialized processes and components for use in synthesizing and assembling diverse structures and materials under biological conditions. Therefore, promising approaches have implemented oligonucleotides [4–7], proteins [8], peptides [9], viruses [10–12], and antibodies [13] as the primary organizational element, with an emphasis on DNA mediated assembly [14]. For example, the tobacco mosaic virus has been used as a scaffold for the selective mineralization of gold nanoparticles along the viral sheath [12]; while antibody–antigen interactions have directed the assembly of antibody functionalized nanoparticles [8]. Other effective interfaces have come to include bifunctional linkers, streptavidin or biotin, and certainly DNA [8]. In DNA mediated assembly, the hybridization of oligonucleotide functionalized nanoparticles has resulted in the formation of binary nanoparticle networks of varying sizes [6], the patterning of gold nanoparticles on DNA modified diatom templates [15], and more recently, the assembly of gold/quantum dot heterostructures with control of the ratio of QDot to gold particles [7]. Consequently, these examples demonstrate the effectiveness of biological interfaces for nanoparticle assembly; however, in none of these systems was there a contribution to nanoparticle synthesis.

Alternatively, small synthetic peptides represent a paragon of biomolecule–nanoparticle interfaces due to the ability to both serve as a template for nanoparticle synthesis and to provide multiple peptides repetitively along a nanoparticle surface. This arrangement of peptides essentially creates an

*Corresponding author. E-mail: Rajesh.Naik@wpafb.af.mil

ISSN 1061-0278 print/ISSN 1029-0478 online © 2006 Taylor & Francis
DOI: 10.1080/10615800600658925

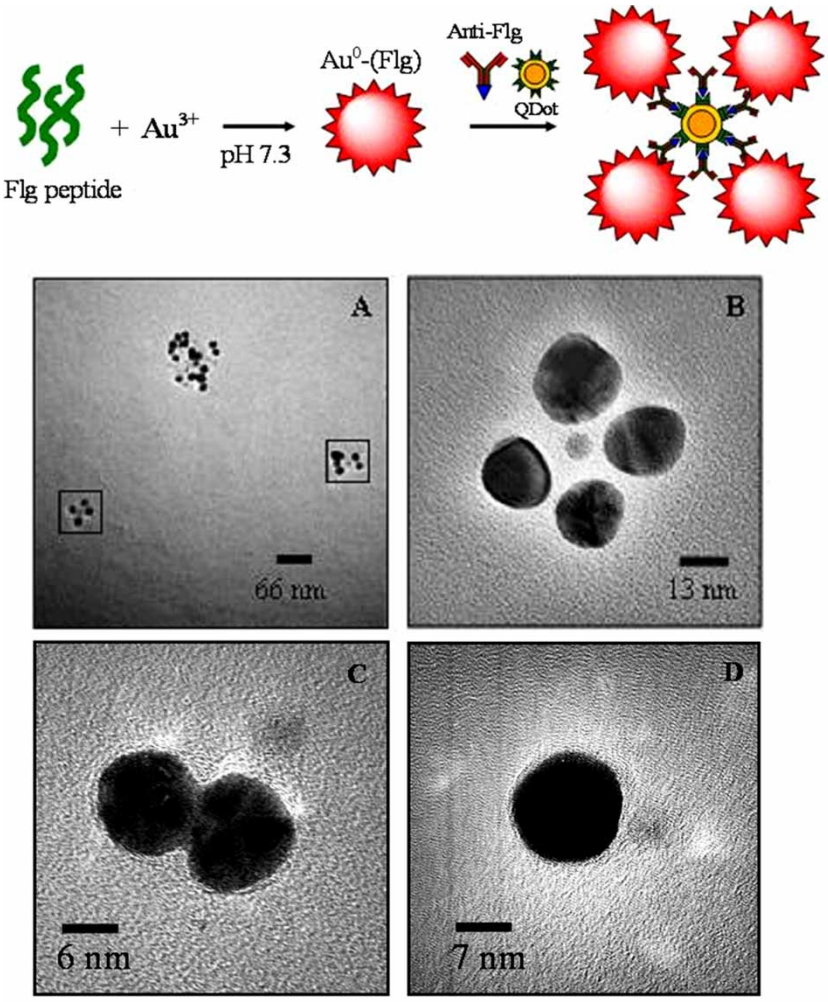

FIGURE 1 Antibody mediated assembly scheme for Qdot/gold structures. Assembly begins with addition of Anti-Flg BioM2 to streptavidin coated quantum dot particles to form an antibody/nanoparticle keystone complex. This is followed by addition of purified Flg gold particles and recognition through the Flg interface. Bottom: TEM micrographs of hybrid nanostructures (A) Au^0-(Flg)/QDot distribution. Square indicates 4 + 1. (B) Au^0-(Flg)/QDot 4 + 1 structure. (C) Au^0-(Flg)/QDot 2 + 1 structure. (D) Au^0-(Flg)/QDot 1 + 1 structure.

immunomolecular interface for antibody recognition and a basic building block for the inspired design of nanoparticle assemblies. To date, immunogenic nanoparticle systems (Au^0, Ag^0, Pt^0, ZnS) possessing peptide epitopes are limited to those displaying histidine-rich peptides (HRE) [16] discovered from the histidine-rich protein II of the malarial parasite *P. falciparum* and the simple tripeptide glutathione [17]. For example, HRE encapsulated nanoparticles were shown to elicit an antibody response from monoclonal antibodies through a commercially available antigen capture assay for malaria. As a result of this pioneering work, other potential epitopes are desired. In particular, the Flg peptide (Asp–Tyr–Lys–Asp–Asp–Asp–asp–Lys) is used as an epitope tag for fusion proteins, contains nanoparticle stabilization amino acid groups, and tyrosine residues attributed to gold reduction; and consequently, represents an excellent peptide template. Herein, we demonstrate the utility of this peptide for the synthesis of gold and silver nanoparticles, antibody recognition, and assembly of hybrid nanostructures with a collection of complementary biological macromolecules as a model system for controlling higher order assemblies (Fig. 1).

RESULTS AND DISCUSSION

As a basis for assembly, the Flg peptide was examined for gold reduction activity, nanoparticle formation, and antibody recognition. The addition of $AuCl_4^-$ to solution containing the Flg peptide resulted in the formation of gold nanoparticles as observed by color changes, plasmon resonance peaks, and transmission electron microscopy [18]. The control hexatyrosine peptide displayed a λ_{max} of 534 nm. Furthermore, since tyrosine is a prominent feature of this peptide set and implicated in gold reduction, we examined the fluorescence of tyrosine over the course of gold formation. As anticipated,

the tyrosine fluorescence from the gold reducing peptide set was quenched upon addition of gold to various extents. Similar gold activity and quenching was previously demonstrated by tyrosine containing viruses [19], proteins [20], and peptides [18,25]. For the tetramer peptide of aspartic acid which lacks critical tyrosine residues; little or no gold nanoparticle synthesis was observed.

TEM analysis of the Flg synthesized gold nanoparticle products revealed a representative range of sizes and structures. The Flg peptide yielded particles with an average size of 13.3 ± 7.4 nm; while examination of the products showed that particles were predominantly spherical in appearance with varying degrees of irregularity and aggregation. Selected area electron diffraction of nanoparticle samples showed a high degree of crystallinity.

The antibody recognition of the Flg epitope was determined using a fluorescence based method [22–25]. The results indicate recognition of particles coated with Flg as demonstrated by fluorescence quenching (Supplementary Material). This parallels the immunomolecular mediated recognition efficiency (25–60%) obtained for the assembly of a superparamagnetic Fe_3O_4-IgG/noble metal nanocluster heterostructure [17]. The lower quenching efficiency is likely due the increased distance between quencher (Au^0 particle) and fluorophore and/or low antibody binding. Based on a descriptive model for phytochelatin encapsulated CdS nanoclusters, we predict that approximately 30–40 peptide ligands envelope the nanoparticle surface of Flg coated gold nanoparticles. Additionally, the Flg peptide coat was confirmed by zeta potential measurements and IR spectroscopy [18].

Given the Flg epitope is readily recognized by antibodies with high specificity, gold/QDot (CdSe/ZnS) nanostructures were sequentially assembled from a group of biological matching components according to the general scheme in Fig. 1. These individual components and their counterparts include biotinylated antibodies to Flg (Anti-Flg BioM2), streptavidin coated quantum dots (QDot-(strept)) with 5–10 streptavidins/QDot (manufacturers specifications), and purified Au^0-(Flg) nanoparticles. From the collection, streptavidin coated nanoparticles (CdSe/ZnS) were incubated with biotinylated Flg antibodies to form the basic keystone structure for assembly. Presumably, the quantum dot streptavidin conjugate has captured approximately 6 biotinylated antibodies at the nanoparticle surface through streptavidin/biotin binding due to the 4 nm diameter of streptavidin molecules and the 7.5 nm diameter of the quantum dot core. This as a result limits the maximal number of Au^0-(Flg) nanoparticles that the keystone complex can accommodate.

Addition of purified Au^0-(Flg) nanoparticles to the QDot-(strept)/Anti-Flg BioM2 structure led to the mediated assembly of remarkable hybrid nanostructures (QDot/Au^0-(Flg)); whereas, addition of gold nanoparticles coated with another Au3 peptide that are not recognized by antibody resulted in an absence of assembly. Under TEM, the assembled products with Au^0-(Flg) as the construction material, showed a distribution of arrangements around the quantum dot center (Fig. 1A). These consisted of predominantly 4 $Au^0 + 1$ QDot, $2 + 1$, and $1 + 1$ structures (Fig. 1B–D) at a frequency of approximately 9%, 28%, and 42% for QDot/Au^0-(Flg) (Fig. 2A). In addition, we analyzed this distribution by

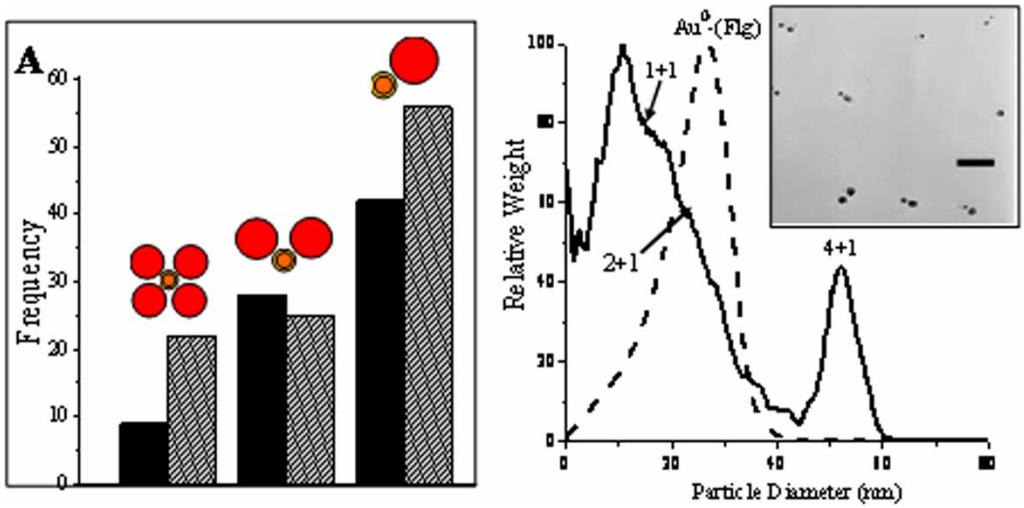

FIGURE 2 (A) Histogram showing frequency of Au^0-(Flg)/QDot assemblies by TEM (black bars) and by sedimentation (grey). (B) Particle size distribution of total assembly population from sedimentation using CPS disc centrifuge particle size analyzer. Calibrated against 377 nm PVC standard. Au^0-(Flg) indicates only gold nanoparticles (dotted line). The peaks are labeled as to particular structure ($4 + 1$, $2 + 1$, or $1 + 1$) of Au^0-(Flg)/QDot according to theoretical diameters. (Inset shows enrichment of $2 + 1$ structures after separation. Scale bar represents 40 nm.)

sedimentation of the total population of assemblies using a CPS disc centrifuge particle size analyzer. This technique applies light scattering to detect different sized particles separated on a sucrose gradient; and as a result, provides statistically accurate sizes, excellent resolution of particles that differ in size by as little as 2%, a large dynamic range, and representation of total nanoparticle population. From the particle size profile, the 4 + 1 structures with a peak maximum weighted around 53 nm (actual size by TEM of 52 nm) were completely resolved from the 1 + 1 and 2 + 1 assemblies (Fig. 2B). Unfortunately, the poor resolution of the 2 + 1 and 1 + 1 are due to the ellipsoidal nature of the assemblies under centrifugation. Comparitively, the frequencies of each assembly in the total population are similar to those determined by TEM. The resultant distribution of assemblies is most likely the preferred arrangements as there is an excess of gold-Flg particles and a variety of Flg epitope conformations on the gold surface. Conversely, at an 8-fold lower concentration of gold, we observed multiple quantum dot satellite particles around the perimeter of gold; and as the concentration was increased from 0–80 mM, a broad distribution of assemblies was favored as observed above.

Notably, these distributions are similar to those obtained from DNA mediated assembly [7]. However, in contrast to DNA mediated assemblies, we obtained fixed geometries around the quantum dot core due to the rigid nature of the antibody/nanoparticle interface. In the 4 + 1 resolved structure (Fig. 1B), four Au^0-(Flg) particles (18–23 nm) are arranged in a distorted tetrahedron with respect to the QDot (7.5 nm ZnS/CdSe core shell, 10–15 nm total diameter which includes polymer surface coating and streptavidin moieties per manufacturers specifications). Dimensionally, the 4 + 1 structure has interparticle spacings (edge to edge) of 1.7 nm and 5.0 nm per Au^0-QDot pair and angles of 80°, 75°, 85°, and 118° consistent with the additive contribution of the streptavidin/biotin/antibody interface as well as a projected tetrahedral geometry. The composition of the 4 + 1 structure was confirmed by energy dispersive X-ray spectroscopy as to the elemental weight % of Au, Zn, and S. The CdSe shell was virtually undetectable due to its low abundance. EDS analysis of several structures revealed 80.05 ± 3.49% Au, 13.84 ± 2.52% Zn, and 6.10 ± 1.06% S or a 1.1:1.0 atomic ratio of Zn:S and four times as much gold to zinc/sulfur.

Optical Characterization

Characterization by absorbance and fluorescence spectroscopy revealed a shift in the plasmon resonance by +14 nm for Au^0-(Flg) and fluorescence quenching of the quantum dot upon assembly and close contact between Au and QDot's. It is speculated that the distance between gold and QDot, size of gold, and number of gold particles will likely determine whether the fluoresence will be quenched or enhanced; and consequently, there is a discrete boundary towards observing one phenomenon over the other. For example, Kotov et al. observed significant enhancement in luminescence of CdTe nanowires coated with gold particles [27], while the fluorescence of CdSe quantum dots was quenched by 80% when attached to a set of gold particles [27]. In our system, we obtain a distribution of structures with 1 to 4 gold particles per quantum dot and an overall quenching of fluorescence of 88.1% (Fig. 3A). To deconvolute the contribution of each structure on fluorescence, we performed a concentration dependence study and theoretical calculations. Experimentally (Fig. 3B), as the concentration of Au^0-(peptide) increased from 0–80 mM, the magnitude of quenching increased (fluorescence decreased). At lower concentrations (<20 mM), the

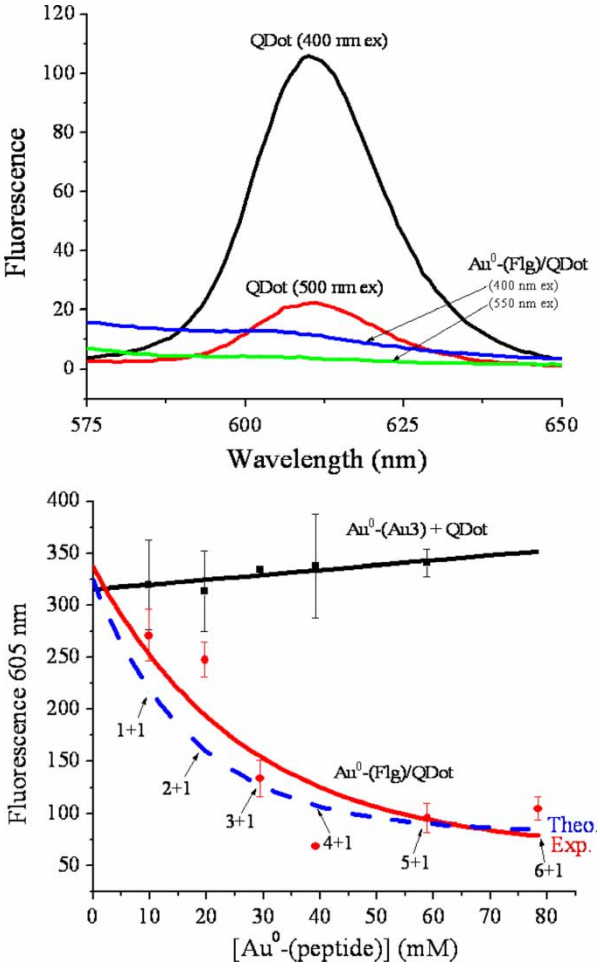

FIGURE 3 (Top) Fluorescence spectra of Au^0-(Flg)/QDot (total population). Excited at 400 nm and at 550 nm. (Bottom) Fluorescence vs. Au^0-(Flg) concentration from 0–80 mM with a fixed QDot concentration of 2 nM. Excited at 400 nm, while fluorescence intenstiy was measured at 605 nm. Negative control was Au^0-(Au3). Also included is the theoretical fluorescence quenching calculated using an absolute number of (1–6) gold particles to one quantum dot.

contribution of gold on fluorescence is entirely due to one or two assemblies, but at higher concentrations, there is an equal contribution towards quenching from many additional structures. The fluorescence profile also correlates with the absolute addition of sequential gold particles and theoretically calculated fluorescence quenching. The dotted curve in Fig. 3 (lower panel) was calculated assuming that the time of exciton-energy transfer from the CdSe-QDot to Au-QDot (γ_{QDot}) is 22 ns. To obtain the theoretical curve in Fig. 4, we described the fluorescence intensity as a function of the number of attached Au-QDots ($N_{\mathrm{Au-QDots}}$) by a simple formula:

$$I_{\mathrm{emiss}}(N_{\mathrm{Au-QDot}},\omega_{\mathrm{emiss}})=\frac{\gamma^0_{\mathrm{rad}}\cdot I^0_{\mathrm{abs}}}{\gamma^0_{\mathrm{tot}}+N_{\mathrm{Au-QDots}}\cdot\gamma_{\mathrm{QDot}}(\omega_{\mathrm{emiss}})}, \tag{1}$$

where $\gamma_{\mathrm{QDot}}=22$ ns is the exciton-transfer rate due to a single Au-QDot and $\gamma^0_{\mathrm{tot}}=1/(11\,\mathrm{ns})$ is the recombination rate in the absence of Au-QDots; I^0_{abs} is the exciton absorption rate of a CdSe QDot in the absence of the Au subsystem. The details of calculation are given in the supplementary material. The formula (1) describes the suppression of fluorescence due to exciton transfer from a QDot to Au nanoparticles and is valid in the absence of the electromagnetic-field enhancement effect (see supplementary material). The latter is a good approximation for our complexes with relatively small number of Au Qdots [30].

Theory

In the next step we will estimate theoretically the important parameter γ_{QDot}. To do this, we employ the fluctuation-dissipation theorem [31] and dipole approximation (see Supplementary material). Then, we arrive to the equation:

$$\gamma_{\mathrm{QDot}}(\omega_{\mathrm{exc}})=-\frac{2}{\hbar}\frac{e^2\cdot\langle r^2_{\mathrm{CdSe}}\rangle_T\varepsilon_{\mathrm{w}}}{d^6\varepsilon^2_{\mathrm{eff}}}R^3_{\mathrm{Au}}2\cdot\mathrm{Im}\left[\frac{\varepsilon_m(\omega)-\varepsilon_{\mathrm{w}}}{\varepsilon_m(\omega)+2\varepsilon_{\mathrm{w}}}\right], \tag{2}$$

where $\varepsilon_{\mathrm{eff}}=(2\varepsilon_{\mathrm{w}}+\varepsilon_{\mathrm{CdSe}})/3$, $\varepsilon_{\mathrm{CdSe}}=6$, and $\varepsilon_m(\omega)$ is the Au dielectric constant; $\varepsilon_{\mathrm{w}}=1.7$ is the dielectric constant of the matrix (water), $\langle r^2_{\mathrm{CdSe}}\rangle_T$ is the squared inter-band optical dipole moment, and $\langle\ldots\rangle_T$ means the thermal averaging. Our theoretical model also incorporates geometrical parameters of the complex, such as the bio-linker length Δ, QDot radii $R_{\mathrm{Au(CdSe)}}=6.5$ nm(3.75 nm), and inter-QDot distance $d=\Delta+R_{\mathrm{Au}}+R_{\mathrm{CdSe}}$ (see Fig. 4, Insert). We now take overall realistic parameters: $\Delta=10$ nm, $d=20.25$ nm, and the Au-constant $\varepsilon_m(\omega)$ from ref. [32]. With Eq. (2), we obtain the experimentally-measured number $\gamma_{\mathrm{QDot}}(\omega_{\mathrm{exc}})=1/(22\,\mathrm{ns})$ if we choose the inter-band optical dipole $\sqrt{\langle r^2_{\mathrm{CdSe}}\rangle_T}=2.16$ Å that is a typical dipole moment for the CdSe nanocrystals. We also can estimate the dipole moment from the measured radiative recombination rate $\gamma^0_{\mathrm{rad}}\approx\gamma^0_{\mathrm{tot}}=1/(11\,\mathrm{ns})$ and obtain an estimate $\sqrt{\langle r^2_{\mathrm{CdSe}}\rangle_T}=2.72$ Å. This is not far from the previous estimation coming from the inter-QDot energy transfer. To obtain an estimate for γ^0_{rad}, we regarded a CdSe QDot as a two-level quantum emitter and used the results of ref. [33]:

$$\gamma^0_{\mathrm{rad}}=\frac{8\pi\sqrt{\varepsilon_{\mathrm{w}}}\omega^3_{\mathrm{exc}}e^2\langle r^2_{\mathrm{CdSe}}\rangle_T}{3(\varepsilon_{eff}/\varepsilon_{\mathrm{w}})^2h\cdot c^3}.$$

It is also interesting to see how $\tau_{\mathrm{exc}\to\mathrm{metal}}=1/\gamma_{\mathrm{QDot}}(\omega_{\mathrm{exc}})$ depends on the exciton energy $\hbar\omega_{\mathrm{exc}}$ (Fig. 4). Since the exciton energy of a semiconductor QDot depends on its size, exciton-energy transfer in hybrid semiconductor-metal complexes can be tailored by choosing appropriate sizes of semiconductor nano-colloids.

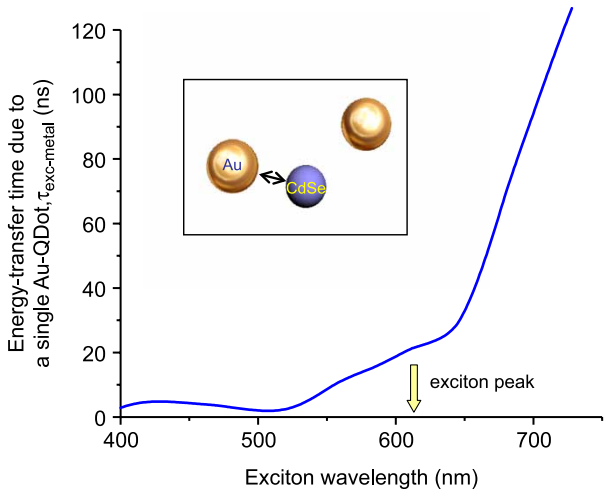

FIGURE 4 Calculated time of energy transfer from a CdSe/ZnS QDot to a single Au-QDot as a function of the exciton wavelength $\lambda_{\mathrm{exc}}=(2\pi\cdot c)/\omega_{\mathrm{exc}}\cdot\sqrt{\langle r^2_{\mathrm{CdSe}}\rangle_T}=2.16$ and $\Delta=10$ nm The other parameters are specified in the text.

CONCLUSION

We have shown the utility of peptides as a template for gold nanoparticle synthesis, stabilizing ligands, recognition element, and building blocks for assembly. As selected, the total set of tyrosine containing peptides actively potentiated the reduction of gold to form peptide stabilized nanoparticles, while the Flg particles were readily recognized by monoclonal antibodies by presenting an immunogenic surface for antibody recognition. This also afforded the requisite interface for the design of higher order structures assembled entirely from biological components. The combination of antibody recognition and streptavidin/biotin binding provided a successful approach towards assembling diverse hybrid nanostructures. Moreover, this provides

a general purpose platform for the assembly of dissimilar materials with tunable properties by simply substituting the peptide coat, antibody, the QD core, and/or peripheral Au^0 particles for different metal or semiconductor particles.

EXPERIMENTAL

Materials

The peptide epitope of Flg, hexatyrosine, and DDDD were purchased from Sigma, while the Au3 peptide was previously synthesized [28,29]. Peptides were dissolved in doubly deionized water to yield a peptide concentration of 10 mg/mL. Monoclonal antibodies to the Flg epitope of Anti-Flg M2-Cy3 (labeled with cyanine dye) (Lot 063K9161) and Anti-Flg BioM2 (conjugated with biotin) (Lot 024K9163) were also purchased from Sigma. Antibodies were diluted by 10 fold to provide a working concentration of 100 μg/mL in Tris buffered saline (TBS) (0.5 M Tris, pH 7.4, 0.15 M NaCl). QDot 605 streptavidin conjugate (Lot # 0304–0037) was obtained from Quantum Dot Corp. Streptavidin conjugates were used as received with no further dilution. A 0.1 M stock solution of $HAuCl_4$ (Aldrich) was prepared in doubly deionized water.

Nanoparticle Synthesis

500 μL of HEPES buffer (pH 7.1) was added to a microfuge tube along with 10 μL of peptide (Flg, Au3, DDDD, or YYYYYY) and 2.5 μL of 0.1 M $AuCl_4^-$, and incubated for 1 h. After gold formation, nanoparticles were purified from excess free peptide by 3 repeated cycles of ethanol precipitation and centrifugation. After final centrifugation, the isolated pellet was redissolved in 100 μL of HEPES buffer.

Fluorescence Antibody Binding Assay

500 μL of TBS buffer, 10 μL of Anti-Flg M2-Cy3, and 2 μL of purified nanoparticle (Au^0-(Au3) Au^0-(Flg)) was added to a 1.5 mL disposable Eppendorf cuvette. Samples were scanned at an excitation of 550 nm, emission of 570 nm, excitation slit width of 5 nm, emission slit width 10 nm, 600 V PMT, 10 sec. cycle, and 3600 sec. total run time, on a Varian Cary Eclipse fluorometer.

Antibody Mediated Assembly

For the QDot streptavidin conjugation; 200 μL of TBS, 0.5 μL of QDot 605 streptavidin conjugates, and 10 μL of Anti-Flg BioM2 was added to a microfuge tube and incubated for 1 h. The excess unconjugated antibodies were then removed by placing solution on a streptavidin coated glass slide for 15 min and transferring to a new microfuge tube. To the purified QDot(streptavidin)/Anti-Flg BioM2; 90 μL of purified gold nanoparticle coated with peptide was added and incubated for 1 h. Reaction was continually monitored over 4 weeks for additional assembly; and after 4 weeks, the solid contents were examined.

Nanoparticle and Assembly Characterization

Gold formation was monitored kinetically by UV-Vis for each peptide on a Varian Cary 500 Scan UV-Vis-NIR spectrophotometer. Nanoparticle structures were examined on a Phillips CM200 transmission electron microscope with a field emission gun operating at 200 kV. TEM samples were prepared by pipetting one drop of solution onto a 3 mm diameter copper grid coated with carbon type A film (Ted Pella, Inc.). Additionally, energy dispersive X-ray spectroscopy (EDS) was performed with same samples in TEM mode on single or nanoparticle groups by tilting 15° towards detector and a beam size of 30 nm. Particle sizing was performed using a sucrose gradient on a CPS disc centrifuge particle size analyzer by CPS instruments operating at 24,000 rpm. Gradients were prepared with 24% and 8% w/w sucrose using a gradient maker and detector calibrated with a 377 nm PVC standard.

Acknowledgement

This work was funded by the Air Force Office of Scientific Research (R.R.N.) and Ohio University (A.O.G.). J.M.S. is a National Research Council Post-Doctoral Fellow.

References

[1] Torres de Araujo, F. F.; Pires, M. A.; Frankel, R. B.; Bicudo, C. E. M. *Biophys. J.* **1986**, *50*, 375.
[2] Simpson, T. L.; Volcani, B. E. *Silicon and Siliceous Structures in Biological Systems*; Springer: New York, 1981.
[3] Wang, J. J.; Xu, Y. Z.; Zhao, Y.; Huang, Y. P.; Wang, D. J.; Jiang, L.; Wu, J. G.; Xu, D. F. *J. Cryst. Growth* **2003**, *252*, 367–371.
[4] Storhoff, J. J.; Mirkin, C. A. *Chem. Rev.* **1999**, *99*, 1849–1862.
[5] Li, M.; Mann, S. *J. Mater. Chem.* **2004**, *14*, 2260–2263.
[6] Mucic, R. R.; Storhoff, J. J.; Mirkin, C. A.; Letsinger, R. L. *J. Am. Chem. Soc.* **1998**, *120*, 12674–12675.
[7] Fu, A.; Micheel, C. M.; Cha, J.; Chang, H.; Yang, H.; Alivisatos, A. P. *J. Am. Chem. Soc.* **2004**, *126*, 10832–10833.
[8] Katz, E.; Willner, I. *Angew. Chem. Int. Ed.* **2004**, *43*, 6042–6108.
[9] Ryadnov, M. G.; Ceyhan, B.; Niemeyer, C. M.; Woolfson, D. N. *J. Am. Chem. Soc.* **2003**, *125*, 9388–9394.
[10] Mao, C.; Flynn, C. E.; Hayhurst, A.; Sweeney, R.; Qi, J.; Georgiou, G.; Iverson, B.; Belcher, A. M. *PNAS* **2003**, *100*, 6946–6951.
[11] Lee, S.; Mao, C.; Flynn, C. E.; Belcher, A. M. *Science* **2002**, *296*, 892–895.
[12] Dujardin, E.; Peet, C.; Stubbs, G.; Culver, J. N.; Mann, S. *Nano Lett.* **2003**, *3*, 413–417.
[13] Wang, S.; Mamedova, N.; Kotov, N. A.; Chen, W.; Studer *J. Nano. Angew. Lett.* **2002**, *2*, 817–822.

[14] Storhoff, J. J.; Mirkin, C. A. *Chem. Rev.* **1999**, *99*, 1849–1862.
[15] Rosi, N. L.; Thaxton, C. S.; Mirkin, C. A. *Chem. Int. Ed.* **2004**, *43*, 5500–5503.
[16] Slocik, J. M.; Moore, J. T.; Wright, D. W. *Nano. Lett.* **2002**, *2*, 169–172.
[17] Slocik, J. M.; Wright, D. W. *Biomacromolecules* **2003**, *4*, 1135–1141.
[18] Slocik, J. M.; Stone, M. O.; Naik, R. R. *Small* **2005**, *1*, 1048–1052.
[19] Slocik, J. M.; Naik, R. R.; Stone, M. O.; Wright, D. W. *J. Mater. Chem.* **2005**, *7*, 749–753.
[20] Zhou, Y.; Chen, W.; Itoh, H.; Naka, K.; Ni, Q.; Yamane, H.; Chujo, Y. *Chem. Commun.* **2001**, 2518–2519.
[21] Bhattacharjee, R. R.; Das, A. K.; Haldar, D.; Si, S.; Banerjee, A. *J. Nanosci. Nanotechnol.* **2005**, *5*, 1141–1147.
[22] Gueroui, Z.; Libchaber, A. *Phys. Rev. Lett.* **2004**, *93*, 166101–166108.
[23] Dubertret, B.; Calame, M.; Libchaber, A. J. *Nat. Biotechnol.* **2001**, *19*, 365–370.
[24] Dulkeith, E.; Morteani, A. C.; Niedereichholz, T.; Klar, T. A.; Feldman, J.; Levi, S. A.; van Veggel, F. C.; Reinhoudt, D. N.; Moller, M.; Gittins, D. I. *Phys. Rev. Lett.* **2002**, *89*, 203002–203004.
[25] Li, H.; Rothberg, L. J. *Anal. Chem.* **2004**, *76*, 5414–5417.
[26] Lee, J.; Govorov, A. O.; Dulka, J.; Kotov, N. A. *Nano Lett.* **2004**, *4*, 2323–2330.
[27] Oh, E.; Hong, M.-Y.; Lee, D.; Nam, S. -H.; Yoon, H. C.; Kim, H.-S. *J. Am. Chem. Soc.* **2005**, in press.
[28] Naik, R. R.; Stringer, S. J.; Agarwal, G.; Jones, S. E.; Stone, M. O. *Nature Mater.* **2002**, *1*, 169–172.
[29] Naik, R. R.; Whitlock, P. W.; Rodriguez, F.; Brott, L. L.; Glawe, D. D.; Clarson, S. J.; Stone, M. O. *Chem. Commun.* **2003**, 238–239.
[30] Govorov, A. O.; Bryant, G. W.; Zhang, W.; Skieni, T.; Lee, J.; Kotov, N. A.; Slocik, J. M.; Naik, R. R. *Nano Lett.*, in press.
[31] Platzman, P. M.; Wolf, P. A. *Waves and Interactions in Solid State Plasma*; Academic Press: New York, 1973.
[32] Palik, E. D. *Handbook of Optical Constants of Solids*; Academic Press: New York, 1985.
[33] Yariv, A. *Quantum Electronics*; 2nd ed. John Wiley & Sons: New York, 1975.